Batteries & Supercaps

Research Article
doi.org/10.1002/batt.202300042

Chemistry Europe
European Chemical Societies Publishing

www.batteries-supercaps.org

Impact of Aluminium Electrode Potential during Charging on Aluminium-Ion Battery Performance with TEA-$AlCl_3$ Electrolyte

Charan Mukundan,[a] Martin Eckert,[a] and Jean-Francois Drillet*[a]

In aluminium (Al) symmetric cell, potentials during Al deposition on an Al foil at 1 mA cm^{-2} were 60–70 mV higher in TEA-$AlCl_3$ electrolyte compared to those measured with EMIMCl-$AlCl_3$ reference. Because of higher electrochemical stability of TEA-$AlCl_3$ solution, cut-off voltage of charging step in AIB full-cell was set to 2.45 V compared to 2.40 V for the reference cell. During long-term cycling at 1 A g^{-1}, the specific capacity of the AIB cell employing TEA-$AlCl_3$ increased from 60 to 94 mAh g^{-1} (57 %) after 1000 cycles while that of cell with EMIMCl-$AlCl_3$ was quite constant at about 60 mAh g^{-1}. This behaviour was explained by continuous decreasing in Al electrode potential at End-of-Charge state (EOC) during deposition reaction (charging step) in TEA-$AlCl_3$ allowing an increase in graphite electrode potential and consequently in AIB cell capacity over the whole experiment. This increase in capacity was accompanied by a raise of defect sites in graphite material.

Introduction

In the last decade, market of lithium-ion battery (LIB) technologies expanded continuously due to huge demand of energy storage solution for consumer, on-grid as well as for transportation applications.[1] However, due to the limited resource and increasing price of lithium and cobalt, battery technologies based on more abundant metals such as Na, Al, Zn, Mg, K and Ca with higher gravimetric energy density are receiving significant attention.[2] Among these metals, Al offer many advantages like high theoretical gravimetric energy density (2980 mAh g^{-1}), abundance in earth crust, cheap price, easy handling and recycling. Therefore, aluminium-ion batteries (AIBs) are considered as economical and sustainable alternatives to LIBs.[3]

Various research groups have investigated different aluminium battery configurations[4] based on intercalation of different ionic species like Al^{3+} (into metal oxide cathode, such as V_2O_5),[5] $AlCl^{2+}$ (into into organic cathode,[6] such as PEDOT)[7] and $AlCl_4^-$ (into graphitic cathode, such as graphitic foam).[8] Among all of them, the performance of AIB involving $AlCl_4^-$ anion intercalation process into graphitic cathode is promising in terms of cost, cycle life and rate capability.[9] Lin et al.[8] demonstrated that AIB with a graphitic-foam cathode can deliver a specific capacity of 60–66 mAh g$^{-1}_{graphite}$ for about 5000 cycles even at a high current density of 5 A g^{-1}. Interestingly, performance of AIBs significantly depends on the morphology and the size of graphite particles that influence mechanisms of $AlCl_4^-$ intercalation into the graphite matrix.[10,11] Han et al.[12] compared the performance of four different graphite materials and concluded that graphite size affects the reversibility and kinetics of $AlCl_4^-$ diffusion into graphite electrodes during intercalation/deintercalation processes. They claimed that graphite morphology influences the trapping, diffusion coefficient and mass transfer kinetics of $AlCl_4^-$ intercalation/deintercalation into/from graphite. Some morphological changes in graphite structure might occur during the first charge-discharge steps. Likewise, Wang et al.[13] analysed the influence of surface area, morphology, and crystallinity of different graphite on their performance as AIB cathode material. Among different graphite materials, a flake-shaped, synthetic kish graphite showed the best capacity of 125 mAh g^{-1} at 1 A g^{-1} which was attributed to its crater morphology and larger surface area.

In terms of electrolyte, chloroaluminate ionic liquid (IL) electrolyte mixture made with Lewis acidic aluminium chloride ($AlCl_3$) and Lewis basic 1-ethyl-3-methylimidazolium chloride (EMIMCl) is considered as state-of-the-art for Al-graphite AIBs because of its high stability and long-term performance. On the other hand, EMIMCl is very expensive that increase the overall cost of the AIBs per kWh.[14] To mitigate the cost issue, $AlCl_3$ based ILs made with cheaper Lewis basic ligands should be developed. Recently, works with urea (80 mAh g^{-1}@100 mA g^{-1}),[15,16] triethylamine hydrochloride (TEA) (88 mAh g^{-1}@100 mA g^{-1}),[17] trimethylamine hydrochloride (TMA) (83 mAh g^{-1}@100 mA g^{-1})[18] and acetamide[16] (67 mAh g^{-1}@100 mA g^{-1}) with comparable specific cell capacity were published. Especially, TEA-$AlCl_3$ is of great economical interest since industrial grade TEA is thousand times cheaper than EMIMCl.[17] The first ambient temperature Al-graphite AIB using TEA-$AlCl_3$ electrolyte was reported by Xia et al.[19] that delivered a discharge capacity

[a] C. Mukundan, M. Eckert, Dr. J.-F. Drillet
DECHEMA-Forschungsinstitut
Energy Storage and Conversion Team
Theodor-Heuss-Allee 25, 60486 Frankfurt am Main (Germany)
E-mail: jean-francois.drillet@dechema.de

Supporting information for this article is available on the WWW under https://doi.org/10.1002/batt.202300042

Research Article
doi.org/10.1002/batt.202300042
Chemistry Europe
European Chemical Societies Publishing

and coulombic efficiency (CE) of 104.7 mAh g^{-1} and 78.4%, respectively after 40 cycles at a current density of 15 mA g^{-1}. Similarly, Gan et al.[20] measured a specific capacity of 96 mAh g^{-1} (CE > 99%) at 100 mA g^{-1} using an Al-graphite cell with TEA-$AlCl_3$ electrolyte. Furthermore, AIB with expanded graphite as cathode material in TEA-$AlCl_3$ electrolyte showed a high specific capacity of 101 mAh g^{-1} at 1 A g^{-1} with a capacity retention of 95.5% after 11,500 cycles.[21] The outstanding performance of the cell was attributed to relatively lower exfoliation degree of expanded graphite even after multiple $AlCl_4^-$ intercalation/de-intercalations steps.

A peculiar observation particular to TEA-$AlCl_3$ is the increase in the specific capacity of graphite over long-term cycling. For instance, Dong et al.[21] mentioned that the capacity of expanded graphite increased by 15.6% up to 98.6 mAh g^{-1} at a current density of 1 A g^{-1} in 5000 cycles. Xu et al.[22] observed a jump in capacity of graphene by 59% (from 94 to 150 mAh g^{-1}) after 7000 cycles at 2.5 A g^{-1}. Similarly, the cell capacity with graphene nanoplatelets increased by 65% (from 80 to 134 mAh g^{-1}) while cycling with 1:1.7 TMA-$AlCl_3$ electrolyte at 2 A g^{-1} for over 3000 cycles.[18] In addition, Xu et al.[17] noticed a ~18% increase in the capacity of graphite cathode after 30,000 cycles while cycling at 5 A g^{-1} (from ~95 to 112 mAh g^{-1}) with 1:1.5 TEA-$AlCl_3$ electrolyte. In all these reports, the reason for such an increase in capacity of graphitic cathode in TEA-$AlCl_3$ and TMA-$AlCl_3$ electrolytes is unanimously attributed to the increase in surface area of graphite due to the exfoliation of graphitic cathode because of continuous intercalation/deintercalation process.

The work aims at exploring more in detail the superior performance of an AIB with a natural graphite with relatively high surface area and flaky morphology as intercalation material and 1:1.5 TEA-$AlCl_3$ (1.5 TEA) in comparison to a cell with 1:1.5 EMIMCl-$AlCl_3$ (1.5 Emi) electrolyte as reference by means of systematic evaluation of electrode potential in Al-symmetrical and full-cell experiments. More specifically, the influence of the electrolyte on the Al and graphite electrode potentials at End-of-Charge state (EOC) during charging step is evaluated with respect to Al reference electrode for the first time. The reason for the increase in capacity of AIB with 1.5 TEA during long-term cycling is also analysed.

Results and Discussion

Physiochemical analysis of electrolytes and natural graphite

Theoretical calculation (Figure S1) suggests that the ratio of $AlCl_4^-$ to $Al_2Cl_7^-$ ion concentration, i.e., $n(AlCl_4^-)/n(Al_2Cl_7^-)$ in TEA-$AlCl_3$ and EMIMCl-$AlCl_3$ is equal to 1 at the molar ratio 1:1.5. For technical application, a compromise between conductivity and viscosity must be made due to which $AlCl_3$ concentration ratio in the range between 1.1 and 1.7 are usually considered for the electrolyte synthesis. The molecular structure of EMIMCl, TEA and the images of 1.5 Emi and 1.5 TEA electrolytes used in this study are shown in Figure 1(a) and their density, viscosity and electrical conductivity values

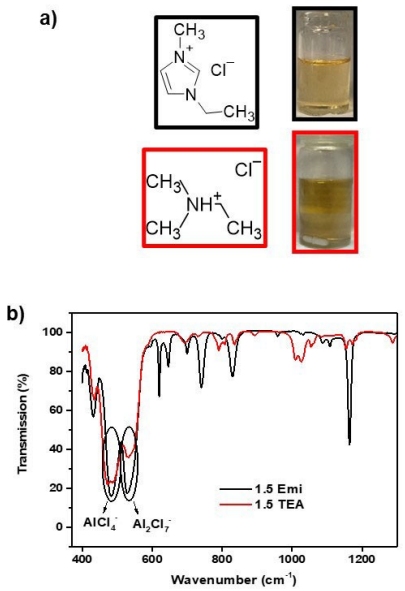

Figure 1. a) Chemical structure of EMIMCl, TEA and images of 1.5 Emi electrolyte (black box), 1.5 TEA electrolyte (red box). b) FT-IR spectra of the electrolytes.

reported in the literature are listed in Table S1. The appearance of 1.5 Emi and as-synthesized 1.5 TEA was light yellowish at room temperature. The characteristic interaction between $EMIM^+/Et_3NH^+$ cations and $AlCl_4^-/Al_2Cl_7^-$ anions (in 1.5 Emi and 1.5 TEA) was analysed by FTIR spectroscopy and respective spectrum is shown in Figure 1(b). Two pronounced peaks observed at 475 and 530 cm^{-1} are attributed to presence of $AlCl_4^-$ and $Al_2Cl_7^-$ anions, respectively while peak intensity reflects the concentration of ionic species.[23] Similarly, the doublet observed at 1080 and 1115 cm^{-1} is induced by $EMIM^+$ cations[24] while stretching vibration between 980 cm^{-1} and 1020 cm^{-1} region corresponds to –NH groups in Et_3NH^+ cations from TEA.[25] Peak intensity related to $AlCl_4^-$ and $Al_2Cl_7^-$ anions are almost equal in 1.5 Emi while in 1.5 TEA the concentration of $Al_2Cl_7^-$ ions is lower than that of $AlCl_4^-$ ions which is an indication for dialuminium heptachloride depletion according to theoretical calculation (Figure S1). The reason for the lower anion concentration in 1.5 TEA is assigned to HCl formation during synthesis causing a loss in chloride ions in the electrolyte. On the other hand, the higher concentration of $AlCl_4^-$ in 1.5 TEA should increase electrolyte viscosity due the strong cation-anion interaction and hydrogen bonding in $[Et_3NH^+][AlCl_4^-]$.[19]

The FESEM images in Figure 2(a) reveals that the natural graphite used in this study has a flaky morphology with an average particle size of 10 µm. From Ar adsorption-desorption isotherm and pore size distribution curve (Figure S2), a specific surface area of 12.17 m^2 g^{-1} with an average pore size ranging between 2 and 15 nm was calculated which denotes a predominant mesoporous structure. The specific surface area of the natural graphite used in this work is comparatively higher than that of other natural, pyrolytic and synthetic graphite materials (up to 9 m^2 g^{-1}).[26] The flaky morphology and

Research Article
doi.org/10.1002/batt.202300042
Chemistry Europe
European Chemical Societies Publishing

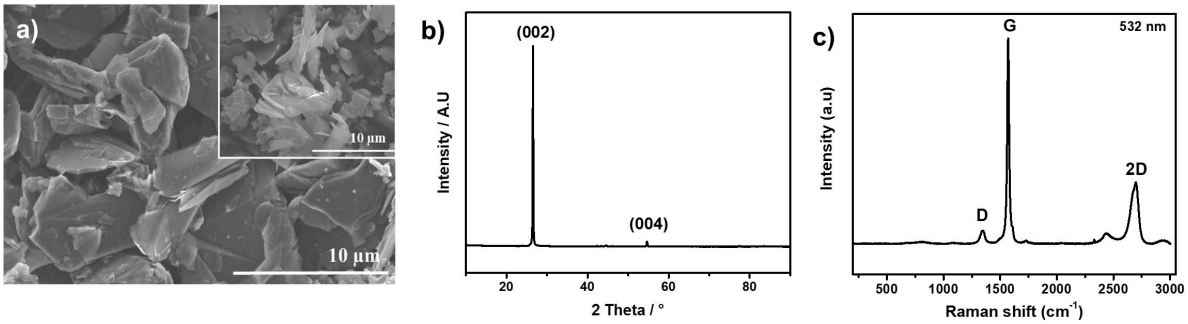

Figure 2. a) FESEM images, b) XRD diffractogram, and c) Raman spectra of natural graphite.

mesoporous structure of the graphite are advantageous since they can improve the electrolyte transport into the graphite structure and enhance electrochemical performance of the AIB.[27] The XRD diffractogram of the graphite (Figure 2b) exhibits a large (002) peak at $2\theta = 26.5°$ and a small (004) one at $2\theta = 54.5°$ which is a characteristic feature for highly crystalline graphite material with the presence of long-range ordering of the graphite layers.[28] The Raman spectra of the graphite sample (Figure 2c) shows characteristic peaks of D, G and 2D bands at around 1360, 1560, and 2710 cm^{-1}, respectively. The I_D/I_G ratio of graphite amounts to 0.06 indicating a high graphitization degree of the material. Relatively high surface area, crystallinity and graphitization degree are desired characteristics for AIB cathode material.[29]

Half-cell measurements

Al deposition/dissolution and $AlCl_4^-$ intercalation/deintercalation reactions were analysed under half-cell condition. The cyclic voltammograms (CV) of aluminium dissolution/deposition in 1.5 TEA and 1.5 Emi electrolytes in Al symmetric cell are shown in Figure 3(a and b). During the first cycle in the cathodic scan two reduction peaks C_2 and C_3 were observed that denotes the bulk deposition of aluminium on the substrate. Correspondingly, the anodic peak A_1 during positive scan represents the subsequent oxidation step resulting in dissolution of the electrodeposited aluminium. On the other hand, peak C_1 start to evolve from cycle 2 induced by underpotential deposition (UPD) of Al which is commonly

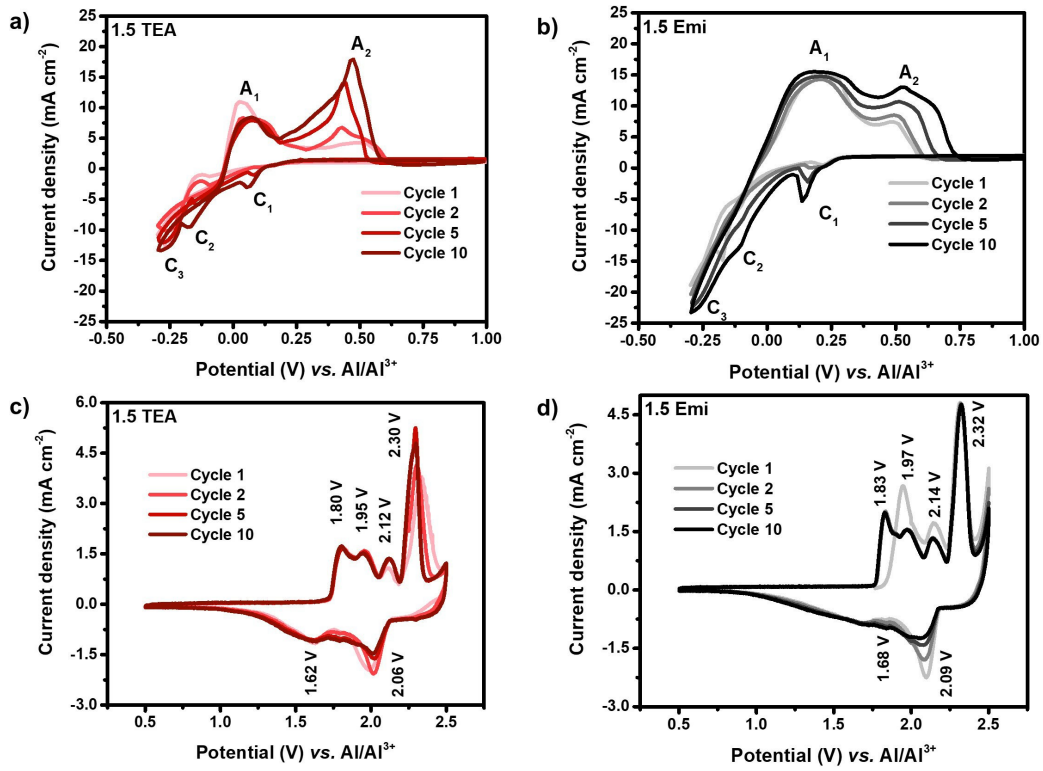

Figure 3. CVs of Al dissolution/deposition reactions on pure Al foil in a) 1.5 TEA, b) 1.5 Emi at 10 $mV s^{-1}$ in Al symmetric cell. CVs obtained in a three-electrode configuration using graphite as working electrode, Al as counter and reference electrode in c) 1.5 TEA, and d) 1.5 Emi within a potential window of 0.5–2.5 V at a scan rate of 1 $mV s^{-1}$.

Research Article
doi.org/10.1002/batt.202300042
Chemistry Europe
European Chemical Societies Publishing

observed during the Al deposition on metals like tungsten (W) and gold (Au).[30,31] The UPD process is attributed to the Al deposition on the trace metals such as Si and Fe (Figure S3 and Table S2) present on the surface of the Al foil. The A_2 peak during the positive scan is assigned to the dissolution of Al UPD. The CVs in Figure 3(c and d) show the electrochemical behaviour of graphite in 1.5 Emi and 1.5 TEA electrolytes up to 10 cycles under half-cell conditions. In both electrolytes, four distinct peaks are clearly visible during anodic scan while only two peaks are well-pronounced in cathodic scan. Each peak observed during the anodic scan (charging process), can be assigned to a change in the graphene layer stacking order resulting from the successive intercalation of $AlCl_4^-$ anions.[32] During the first cycle, a peak localized at 1.80–1.95 V in 1.5 TEA and 1.83–1.97 V in 1.5 Emi at the beginning of charging step is attributed to $AlCl_4^-$ intercalation in every 6th graphene interlayer spacing also known as *stage 6* intercalation. The next oxidation peak at ~2.14 V (1.5 Emi) or ~2.12 V (1.5 TEA) corresponds to *stage 5* intercalation step while the final and significant peak at ~2.30 V (1.5 TEA) and ~2.32 V (1.5 Emi) resulted from *stage 4* intercalation process. The shift of the peak position during the initial cycles correlates to the 'activation' process of graphite in both the electrolytes where the graphite undergoes structural changes due to the partial irreversibility and trapping of the $AlCl_4^-$ anions in the graphite matrix.[33] It can be seen that during the activation process of graphite in 1.5 TEA, the peaks related to *stage 6* intercalation remains unchanged while the intensity and the position of peak related to *stage 5* shifted from 2.10 V to 2.12 V during 2nd cycle and *stage 4* intercalation shifted from 2.33 V in 1st cycle to a lower potential of 2.30 V by 10th cycle. Xu et al.[22] observed similar changes in peak position corresponding to *stage 4* intercalation only in TEA-$AlCl_3$ electrolyte which was attributed to higher charge transfer resistance at electrolyte/electrode interface compared to that in EMIMCl-$AlCl_3$. Consequently, severe stress/strain is caused on the graphene layer during *stage 4* intercalation of $AlCl_4^-$ anions into graphite in TEA-$AlCl_3$ electrolyte. Regardless of these differences, the magnitudes of current density and intercalation/deintercalation steps in 10th cycle were similar in both electrolytes. It is also worthwhile to note that the onset potential of electrolyte decomposition in 1.5 TEA amounts to about 2.45 V which is by 50 mV higher than that in 1.5 Emi indicating a slightly larger electrochemical stability window. Moreover, at the vertex potential of 2.50 V, the current density value of intercalation process into graphite amounts to 1.18 mA cm^{-2} in 1.5 TEA compared to 2.59 mA cm^{-2} in 1.5 Emi. This demonstrates the larger stability window of TEA electrolyte compared to Emi. As a result, cut-off voltage of charging step during galvanostatic cycling of AIB cell was set to 2.45 V in 1.5 TEA and 2.4 V in 1.5 Emi.

Symmetric Al cell

Figure 4(a and b) shows potential vs. time curves of galvanostatic Al stripping/deposition tests at two different current densities. At 0.5 mA cm^{-2}, potential values of Al deposition were 25–30 mV lower in 1.5 Emi compared to those in 1.5 TEA electrolyte while potential values during Al dissolution step were quite similar after 5–10 cycles in both electrolytes. At 1 mA cm^{-2}, potential during the first Al dissolution and deposition step amounts to 200 and 288 mV respectively compared to only 122 and 45 mV in the cell with 1.5 Emi, respectively. After 5 cycles, the potentials of Al dissolution and deposition process in 1.5 TEA reduced considerably by 75 and 67 %, respectively resulting from the significant change occurring on the surface morphology of Al foil.[34] The higher overpotential values observed during Al deposition step in TEA might be due to lower $Al_2Cl_7^-$ ion concentration compared to that in Emi as shown by FTIR study in Figure 1. Notably, irrespective of the current density, the potential during the deposition process was always higher in 1.5 TEA than in 1.5 Emi whereas the potential during Al dissolution was quite identical in both the electrolytes. The higher potential during Al deposition in 1.5 TEA is attributed to higher viscosity and low n($Al_2Cl_7^-$) ion concentration in the electrolyte that results in lower specific conductivity (Table S1). It is noteworthy to mention that the specific conductivity of TEA-$AlCl_3$ electrolyte can be improved by adding organic solvents such as dichloro-

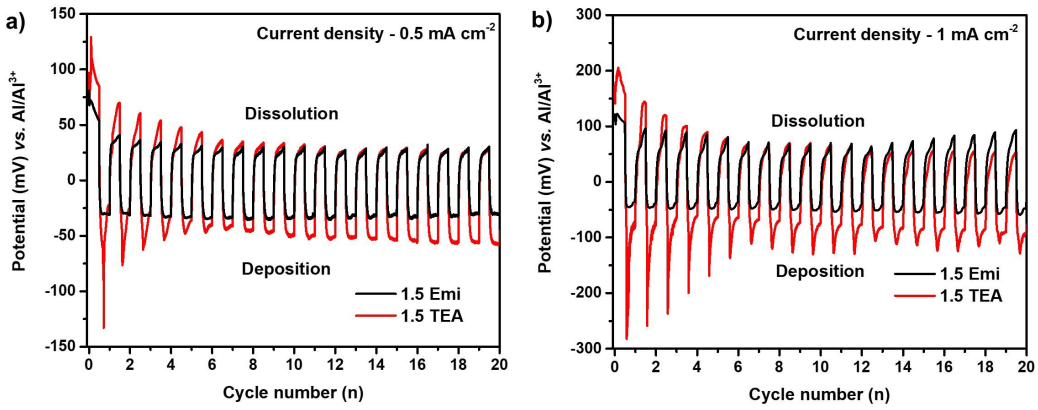

Figure 4. Comparison of potential vs. time curve during galvanostatic cycling of AIB in 1.5 TEA (red line) and 1.5 Emi (black line) for a dissolution/deposition time of 2 hours at RT at a) 0.5 mA cm^{-2} and b) 1.0 mA cm^{-2}.

Research Article
doi.org/10.1002/batt.202300042

methane (DCM) and 1,2-dichlorethane (DCE) that reduces the electrolyte viscosity.[19]

AIB full cell

Activation phase

The influence of the electrolyte on the behaviour of Al-graphite AIBs was evaluated by galvanostatic cycling. Figure 5(a and b) exhibits the charge-discharge behaviour during activation phase under AIB full-cell condition cycled at 100 mA g^{-1}. The curve related to charging process consists of three plateaus which corresponds to three intercalation stages that was observed in CVs. During the 'activation' phase, the specific charge capacity of graphite decreases gradually while the specific discharge capacity increases with cycle number in both electrolytes. The lower CE during initial cycles is attributed to irreversible trapping of $AlCl_4^-$ anions in the graphite structure. After activation period by the end of 25 cycles, CE of AIB in 1.5 TEA jumped to ~97% and the specific capacity is enhanced by 17% to 99 mAh g^{-1} while the specific capacity increased only by 2.5% in 1.5 Emi. The significant improvement in the performance of AIB cell with 1.5 TEA is assigned to quite long activation process up to 10 cycles due to modification in graphite structure.[22]

Rate capability

During rate capability test up to 5 A g^{-1} (Figure 6a–c), AIB shows a better performance with 1.5 TEA electrolyte at all current densities. For instance, the discharge capacity of AIB with 1.5 TEA at 0.1 and 2 A g^{-1} was 98.7 and 46.9 mAh g^{-1}, respectively compared to 87.8 and 43.8 mAh g^{-1} for AIB with 1.5 Emi. At lower current densities ($\leq$0.75 A g^{-1}), the capacity fading of AIB with respect to reference capacity at 0.1 A g^{-1} is gradual in both 1.5 TEA and 1.5 Emi (Table S3). When the current density was higher than 1 A g^{-1}, however, the capacity fading was more pronounced in AIB with 1.5 TEA. For instance, at 5 A g^{-1}, the capacity of AIB amounted to 28.15 and 30.5 mAh g^{-1} while the capacity retention was 28.5 and 34.7% in 1.5 TEA and 1.5 Emi, respectively. Meanwhile, the CE of AIBs in both the electrolytes was lower than 98% until 0.25 A g^{-1} and increases up to 99% from 0.5 A g^{-1}. When the current density was lowered from 5 A g^{-1} back to 0.1 A g^{-1} (blue curve), the specific capacity of AIB cells was identical compared to that of the initial cycle (black curve) in both the electrolytes as shown in Figure 6(a and b).

Long-term stability at 1.0 A g^{-1}

The long-term performance and stability behaviour of AIBs in 1.5 TEA and 1.5 Emi at 1 A g^{-1} for over 1000 cycles is shown in Figure 7(a and b). Interestingly, the specific capacity of AIB in 1.5 TEA increased significantly from 60 up to 87 mAh g^{-1} during first 500 cycles (Figure 7a) and reached a maximum value of 94.2 mAh g^{-1} by 1000th cycle that represents an increase of about 57% compared to that of yielded during the first cycle. In contrast, AIB with 1.5 Emi at 1 A g^{-1} showed a very good cyclic stability with a constant normalized capacity of 62 mAh g^{-1} for over 1000 cycles (Figure 7b) and a capacity retention of 100%. It should be noted that the cells were subjected to temperature fluctuation in the laboratory within the range of 19–22 °C during day-night cycle. The effect of temperature changes on capacity was more pronounced in AIB with 1.5 TEA (~5%) than with 1.5 Emi (~1.5%) (shown in the inserts in Figure 7a and b). As expected, increase in room temperature led to higher specific capacity values due to higher mobility of anions and cations in the electrolyte that results in better utilisation of graphite.[35] Surprisingly, CE values decrease with increasing temperature which can be assigned to slight electrolyte decomposition at higher voltage.[32] After 1000 cycles, capacity of AIB with 1.5 TEA was 52% higher than that in the cell with 1.5 Emi. The charge-discharge curves (Figure 7c) from long-term cycling in 1.5 TEA show that the length of plateau 3 (violet region) during charging step is growing gradually along with the specific capacity that increased from 60 to 94.2 mAh g^{-1} by the end of 1000th cycle.

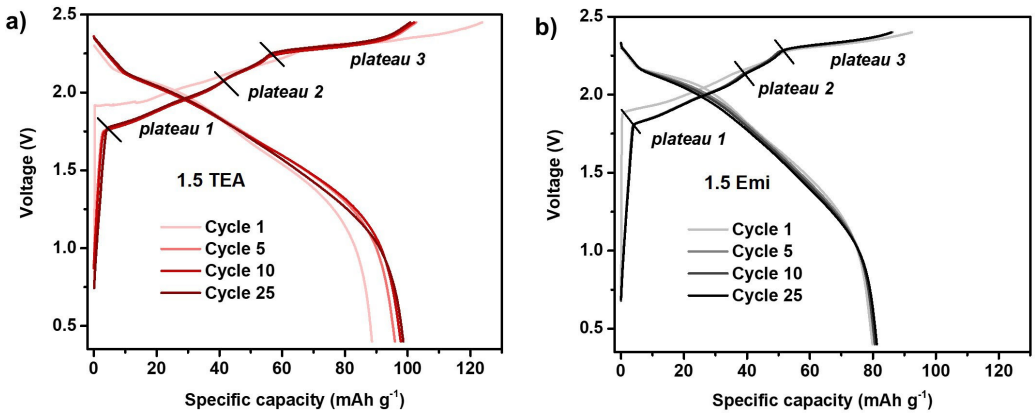

Figure 5. Charge-discharge curves of AIB cycled at 100 mA g^{-1} for the activation of graphite in a) 1.5 TEA and, b) 1.5 Emi electrolyte.

Research Article
doi.org/10.1002/batt.202300042
Chemistry Europe
European Chemical Societies Publishing

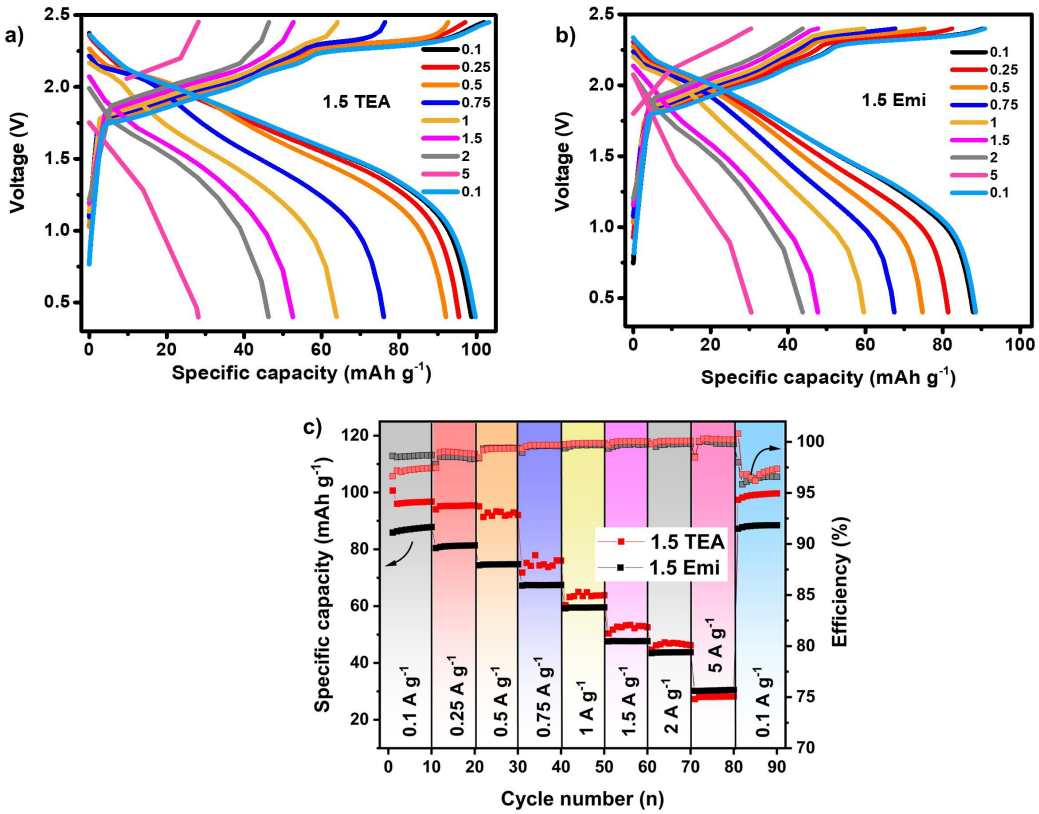

Figure 6. Charge-discharge curves during galvanostatic cycling at different current densities in A g^{-1} in a) 1.5 TEA and b) 1.5 Emi. c) Comparison of specific capacity and current efficiency (CE) of AIB in 1.5 TEA and 1.5 Emi cycled at different current density. The experiments were carried out after 25 activation cycles at 0.1 A g^{-1} shown in Figure 5.

Expectedly, the plateaus in the charge/discharge curves of AIB with 1.5 Emi (Figure 7d) shows no significant changes after 50 cycles. To ascertain the reason for the increasing capacity, we analysed the charge/discharge curves of every 50th cycle and evaluated the capacity contribution of each plateau (plateaus 1 to 3 as shown in Figure 5) at the EOC state during the corresponding charging process. In 1.5 TEA, the cumulative capacity contribution from plateaus 1 and 2 showed a slight increase in capacity from 50 to 57 mAh g^{-1} within 100 cycles and remains constant afterwards (Figure 7e). In contrast, capacity contribution of plateau 3 increases significantly from 10 up to nearly 40 mAh g^{-1} (~400% increase) by the end of long-term cycling representing a 57% increase in overall capacity of AIB in 1.5 TEA. Whereas in 1.5 Emi, capacity contribution of plateaus 1, 2 and 3 as well as the total cell capacity remain constant throughout long-term cycling (Figure 7f). Such a significant fluctuation and increase in capacity in 1.5 TEA which is almost absent in 1.5 Emi can only be the result of electrode/electrolyte reaction that is peculiar to 1.5 TEA electrolyte.

In following section, contribution of Al and graphite electrode potential to AIB cell voltage is discussed more in detail by evaluation of the 3 first (Figure 8a and b) and last (Figure 8c and d) charge-discharge cycles as well as the Al anode and graphite cathode potentials at EOC for all 1000 cycles (Figure 8e and f). The potential vs. time curves related to first 3 cycles of long-term cycling of AIB cell in 1.5 TEA (Figure 8a) shows that when the potential of Al anode reached 50 mV during charging step, it increased within 20 seconds up to 150 mV that leads to a fast jump of cell voltage from 2.25 to 2.45 V. Contrastingly, in 1.5 Emi (Figure 8b) no such sudden increase in Al anode potential was observed resulting in a smooth increase of cell voltage till 2.4 V. Interestingly, during last 3 cycles in 1.5 TEA (998th to 1000th), the increase in potential of Al electrode during charging process was gradual and reached only 80 mV at EOC state which is nearly 2 folds lesser than during initial cycles (Figure 8c). Consequently, the AIB cell voltage also increased smoothly along with the cathode potential that resulted in a higher capacity contribution from plateau 3 same as it was in 1.5 Emi (Figure 8d). To explain possible reason for the difference in capacity between AIB cell using 1.5 TEA and 1.5 Emi, the potential of the Al and graphite electrodes at the EOC state was plotted for all 1000 cycle whereas cut-off voltage of charging step was set to 2.45 and for 2.40 V for AIB cell with 1.5 TEA and 1.5 Emi electrolyte, respectively. From Figure 8e–f, it can be generally observed that fluctuation in both Al and graphite electrode potentials are less pronounced in AIB with 1.5 Emi (< 10 mV) than that with TEA (10–50 mV). The latter can be assigned to a very long activation phase over 200–300 cycles related to some effects such as higher electrolyte viscosity and sensitivity to day-night temperature variation in the lab up to 3 °C.

Research Article
doi.org/10.1002/batt.202300042

Chemistry Europe
European Chemical Societies Publishing

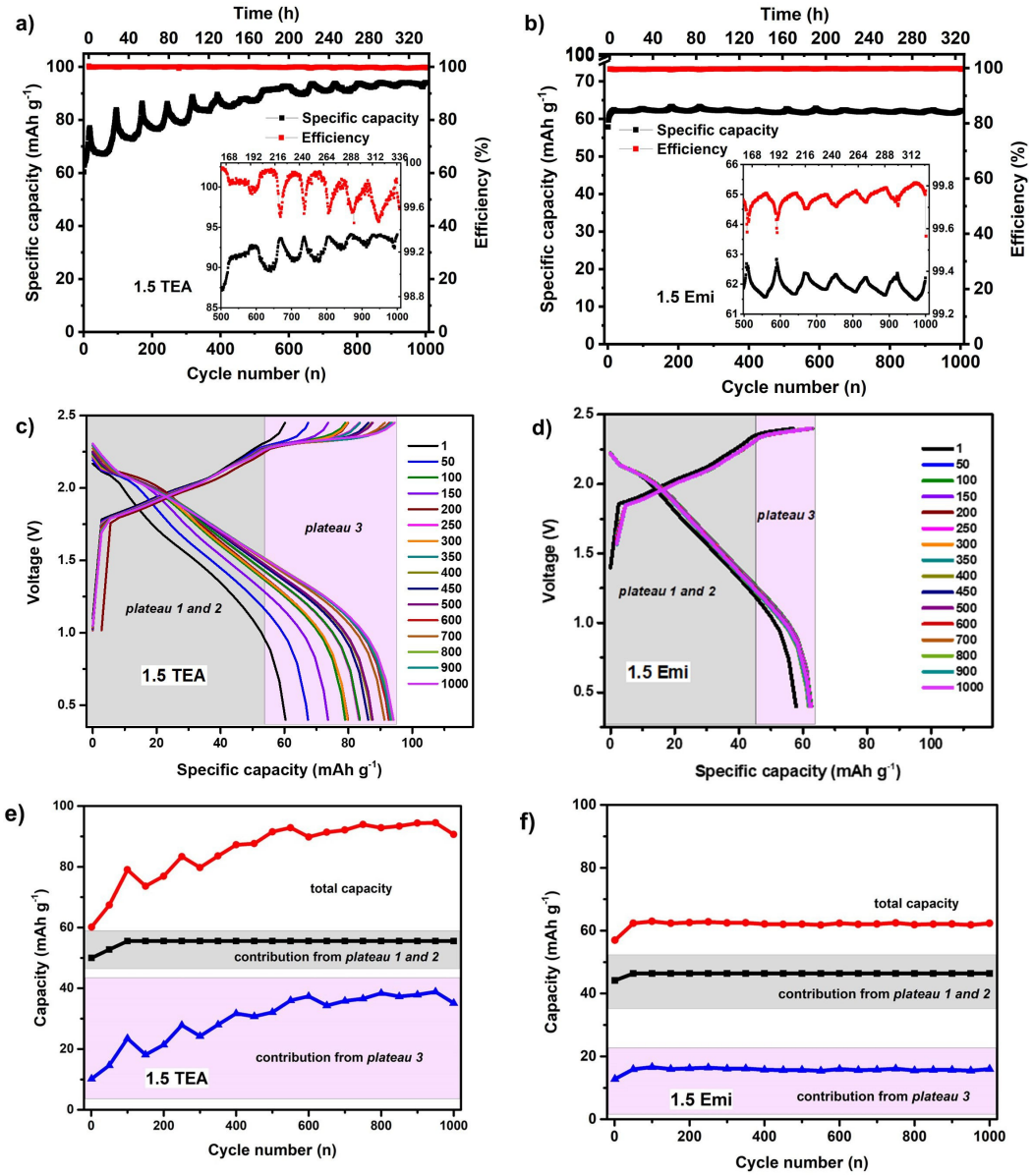

Figure 7. Specific capacity and coulombic efficiencies of AIB with natural graphite in a) 1.5 TEA and b) 1.5 Emi during long-term cycling at 1 $A g^{-1}$ (inlets in the figure shows the magnified view of data in last 500 cycles). Charge-discharge curves of AIB every 50 cycles during long-term cycling at 1 $A g^{-1}$ in c) 1.5 TEA and d) 1.5 Emi and respective capacity contribution from plateau 1 and plateau 2 combined (black line) and plateau 3 (blue line) to the total capacity (red line) in e) 1.5 TEA and f) 1.5 Emi. The experiments were carried out after rate capability studies shown in Figure 6.

From Table 1 it is obvious that the electrolyte nature and higher cut-off-voltage (COV) by 50 mV during charging step in case of cell with 1.5 TEA have a substantial impact on cathode potential at EOC which is nearly 10 mV higher than that in the cell with 1.5 Emi after 1000 cycles.

By contrast, the potential of Al electrode at EOC in 1.5 TEA is at least 42 mV (even up to 107 mV after 50 cycles) higher than that measured in AIB cell with Emi electrolyte over the complete experiment. One possible explanation for the higher potential detected at Al electrode at EOC with 1.5 TEA can be the lower concentration of $Al_2Cl_7^-$ ions in 1.5 TEA electrolyte

Table 1. Al & graphite electrode potentials during different cycle numbers in 1.5 TEA and 1.5 Emi from Figure 8 (e and f).

Average potential @ EOC vs. Al/Al^{3+} [mV]	1 to 50 cyc.	51 to 500 cyc.	501 to 1000 cyc.
Graphite/TEA	2,342 ± 18.8	2,365 ± 9.3	2,372 ± 3.7
Graphite/Emi	2,356 ± 1.4	2,359 ± 1.6	2,364 ± 0.9
Al/TEA	107.7 ± 18.8	86.4 ± 9.3	77.8 ± 3.7
Al/Emi	43.0 ± 1.4	40.5 ± 1.6	35.4 ± 0.9

Research Article
doi.org/10.1002/batt.202300042
Chemistry Europe
European Chemical Societies Publishing

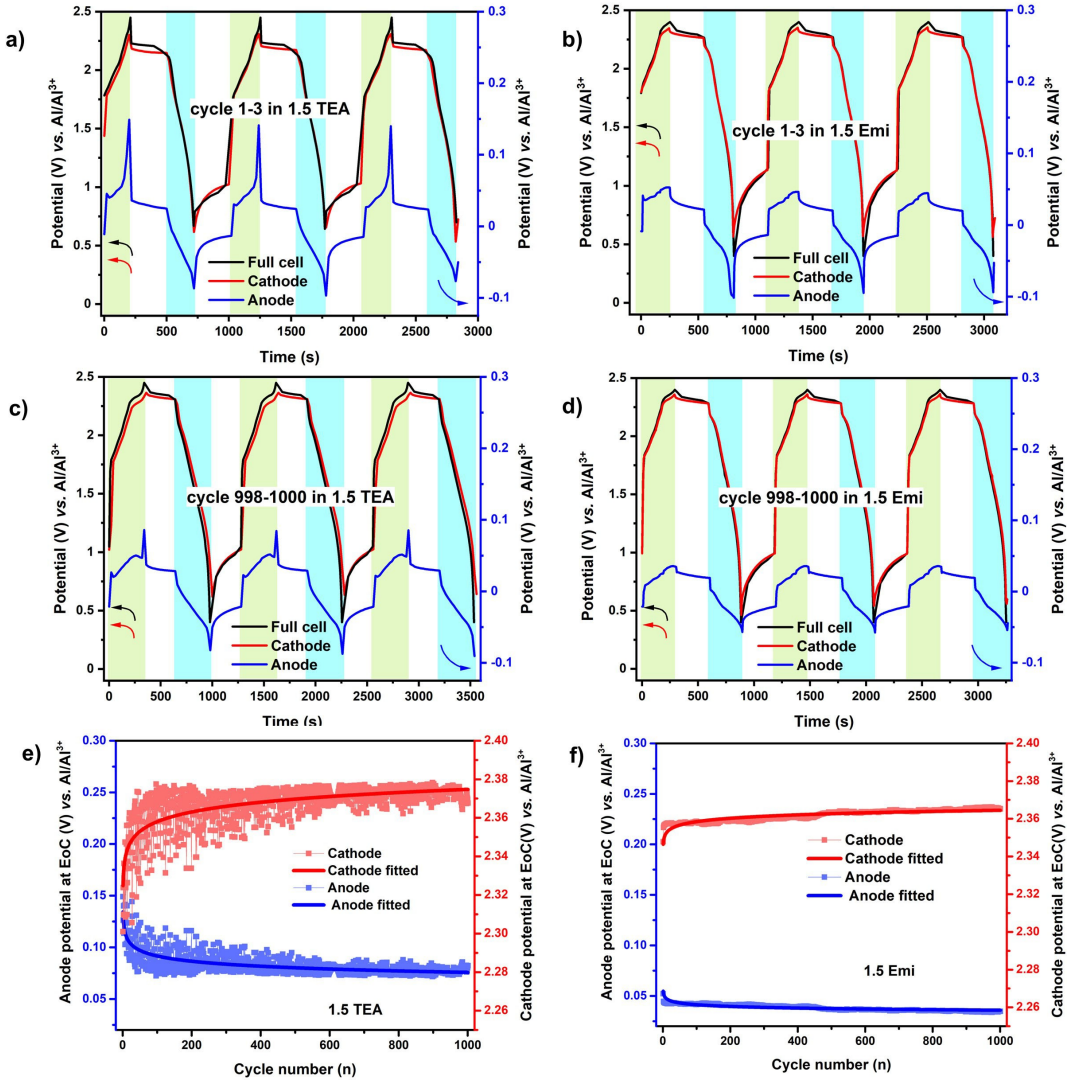

Figure 8. Electrode potential of Al anode, graphite cathode and the corresponding cell voltage during charging (green region) and discharging (blue region) process in first three cycle (1st to 3rd) in a) 1.5 TEA and b) 1.5 Emi as well as the last three cycles (998th to 1000th) in c) 1.5 TEA and d) 1.5 Emi, during long-term cycling at 1 A g^{-1}. Comparison of the potentials of Al and graphite electrode at EoC during long-term cycling at 1 A g^{-1} in e) 1.5 TEA and f) 1.5 Emi. The experiments were carried out after rate capability studies shown in Figure 6.

solution compared to that in 1.5 Emi (see FTIR measurement in Figure 1b) resulting in lower corrosion activity and consequently in difference in Al foil roughness.

In addition, the influence of the long-term cycling in 1.5 TEA and 1.5 Emi on the graphite morphology was characterized by using Raman spectroscopy. Figure 9 shows the Raman spectra of graphite electrode in pristine state and after long-term cycling at 1 A g^{-1}. It is clearly seen that intensity of D and 2D peaks increased significantly after cycling procedure while G peak intensity decreases reflecting the formation of additional defects in the graphite structure. Accordingly, the I_D/I_G ratio increased from 0.06 for pristine graphite to 0.46 and 0.25 for the graphite cycled in 1.5 TEA and 1.5 Emi, respectively. It has been previously reported that a co-intercalation of $EMIM^+$ or Et_3NH^+ cations into the graphite happens during charge-discharge process that induce morphological changes in the graphite structure.[22,33] Similarly, the increase in the I_D/I_G of graphite after cycling can be attributed to the co-intercalation of Et_3NH^+ and $EMIM^+$ cations into the graphite that leads to severe delamination of the graphite particles. However, the higher I_D/I_G ratio of graphite after cycling in 1.5 TEA than in 1.5 Emi is attributed to higher delamination caused by the larger size of Et_3NH^+ cations (128.7 Å) compared to the $EMIM^+$ cations (109.3 Å) as reported by Xu et al.[22] resulting in stronger delamination of graphite matrix. The higher delamination of graphite cycled in 1.5 TEA results in increased surface area of the graphite that allows better diffusion of electrolyte and access to active sites and consequently contributes to an improvement in the specific capacity of the cathode after few hundred cycles.[21,22] The results shows that the increase in capacity of AIBs with 1.5 TEA during long-term cycling is a cumulative effect of the decrease in potential of Al anode and the morphological changes in the

Research Article
doi.org/10.1002/batt.202300042
Chemistry Europe
European Chemical Societies Publishing

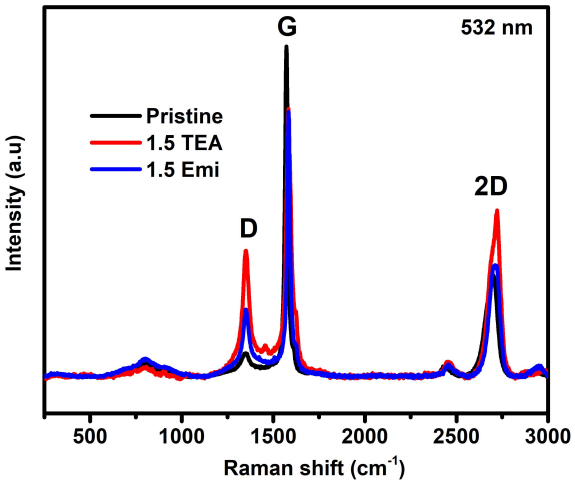

Figure 9. Raman spectra of graphite electrode before and after cycling in 1.5 Emi and 1.5 TEA electrolyte after long-term cycling at 1 $A g^{-1}$.

graphite matrix that results in increase in capacity contribution from plateau 3 in graphite cathode.

Conclusions

In this work, we systematically studied the suitability of 1.5 TEA electrolyte for Al-graphite AIBs focussing more specifically on the effect of the Al and graphite electrode potentials on cell performance in comparison with that of an AIB with 1.5 Emi electrolyte as reference. Our experiments showed that the Al dissolution/deposition process is stable and reversible in both the electrolytes while the potential during Al electrodeposition process was higher in 1.5 TEA. This was assigned to its higher viscosity and slightly lower $Al_2Cl_7^-$ concentration compared to 1.5 Emi. The natural graphite material used in this study showed a high crystallinity and relatively high surface area that allows a reversible, well-defined, and comparable activity for intercalation/deintercalation processes of $AlCl_4^-$ in both the electrolytes. At lower current densities than 0.75 $A g^{-1}$, the capacity of AIB was superior in 1.5 TEA but almost similar in both electrolyte at current density higher than 1 $A g^{-1}$. During long-term cycling experiment in 1.5 TEA at 1 $A g^{-1}$, the Al electrode potential at EOC between 50th and 1000th cycle dropped by about 25% allowing the graphite material to undergo intercalation process up to about 2.375 V compared to 2.365 V for the cell with 1.5 Emi. After 1000 cycles, the capacity of AIB with 1.5 TEA at 1 $A g^{-1}$ was 94.5 $mAh g^{-1}$, which is 52% higher than it was in 1.5 Emi (62 $mAh g^{-1}$). The significant increase in the capacity of AIB with 1.5 TEA was found to be the result of the decrease in the Al anode potential as well as morphological changes in the graphite cathode. Firstly, the increase of defect sites in graphite crystal structure evidenced by Raman investigation. Secondly, the decrease in potential of Al electrode after few hundred cycles evidenced by the potential of Al anode and graphite cathode at EOC. These results clearly illustrate that TEA-$AlCl_3$ is a promising, relatively low-cost, and a highly performing alternative to EMIMCl-$AlCl_3$ electrolyte for AIBs.

Experimental Section

Chemicals and cell components

Natural graphite powder (Micro Graphite 10 my 96, 99.9%, ~10 μm, Prographit, Untergriesbach, Germany), $AlCl_3$ (99.999%, granules, Acros), 10 wt% polytetrafluoroethylene suspension (PTFE, 10 wt% in H_2O, Quintech, Göppingen, Germany), and Dimethyl carbonate (98% purity, Iolitec, Heilbronn, Germany) were used as received. Al foil (thickness in 200 μm, 99.5%, ChemPUR), W and Mo rod (Ø = 10 mm, 99.999%, HMW Hauner, Röttenbach, Germany), Glassy carbon rod (Ø = 10 mm, Supporting InformationGRADUR®, HTW, Thierhaupten, Germany) were thoroughly washed with isopropanol and dried before the use. GF/D (650 μm in thickness, Whatman™/Cytiva, Freiburg, Germany) was dried at 105 °C under vacuum and transferred to the glovebox (UniLabPro, $H_2O/O_2 <$ 0.1 ppm, MBraun, Garching, Germany). Triethylamine hydrochloride (98%, Acros) was dried at 70 °C under vacuum for 48 h. EMIMCl-$AlCl_3$ of molar ratio 1:1.5 (98% purity, Iolitec, Heilbronn, Germany) electrolyte was used as received.

Preparation of TEA-$AlCl_3$ electrolyte

10 g of 1:1.5 TEA-$AlCl_3$ electrolyte was prepared by slowly adding 5.923 g of $AlCl_3$ to 4.076 g of TEA and stirring in an argon-filled glove box ($O_2 < 1$ ppm, $H_2O < 1$ ppm) at ambient temperature.

Preparation of graphite electrode

Desired mass of graphite and PTFE suspension was mixed in a 90:10 weight ratio in a H_2O: isopropyl alcohol solution (8:2 volume ratio). The graphite slurry was mixed using Ultra-Turrax® (T-18, IKA, Staufen, Germany) at 18000 rpm for 15 min followed by 5 min sonication until a homogeneous dispersion was obtained. The obtained dispersion was spray-coated on one side of 8×8 cm Whatman GF/A glass fiber. The electrode was dried at 60 °C in a hot air oven (ROK 3/30, W. C. Heraeus, Hanau, Germany) to remove the residual solvent which was later cut into Ø = 9 mm disks. The electrodes were dried under vacuum at 0.1 mbar and 105 °C overnight using a self-built Schlenk-line apparatus and subsequently moved into glovebox for further use. The average active mass loading of graphite in the electrode was in the range of 3–4 $mg cm^{-2}$.

Physicochemical characterization

Attenuated total reflectance Fourier transform infrared spectra (ATR-FTIR) of electrolytes were recorded in the scan range of 400–1500 cm^{-1}, with a resolution of 4 cm^{-1} using spectroscopic meter (iS50 Nicolet, Thermo Scientific Instrument Co). The morphology of the graphite powder was obtained using a FESEM (4100 Hitachi, Tokyo, Japan) at 20 mm WD and 20 kV power. The structural proprieties of the graphite powder were investigated by X-ray diffraction (XRD) (D8 Advance, BRUKER, Karlsruhe, Germany) with Cu K_α radiation (0.154 nm) in the 2θ range from 10° to 90° with a step size of 0.018°. Raman spectra of graphite electrode was measured with a confocal Raman microscope (InVia Reflex, Renishaw, Pliezhausen, Germany). The laser beam (532 nm) was focused through a 50× objective lens (DM 2500, Leica, Mannheim, Germany) with ~1 mm spot size. A single spectrum consisted of 20

accumulated scans with an acquisition time of 20 s each. The background signal was subtracted using the baseline correction mode. Prior to the Raman analysis, the cycled electrodes were washed removed from the cells inside glovebox and were washed thoroughly with Dimethyl carbonate solution and was later dried to remove the residual electrolyte. Pore structure of graphite was determined with argon at 87 K using physisorption technique (Autosorb iQ, Station Quantachrome/3P Instruments, Odelzhausen, Germany).

Cell Fabrication

The test cells with 2-electrodes or 3-electrodes made of PTFE (Swagelok®) with an internal diameter of φ 10 mm was used. All the cells were assembled in an argon-filled glovebox. For Al-graphite cells, Al foil (φ 10 mm) was used as anode or counter electrode and graphite electrode (φ 9 mm) was used as cathode or working electrode. For Al-Al symmetric cells, Al foil (φ 10 mm) was used as working as well as counter electrode. Mo rods (φ 10 mm) were used as current collector. For 3-electrodes cells, Al rods (φ 6 mm) were used as reference electrode. 2 layers of GF/D (φ 10 mm) was used as separator for all the cells. The cells were filled with excess electrolyte to ensure that the capacity of cathode is not limited by the concentration of $AlCl_4^-$ present in the electrolyte. To study the stability of glassy carbon, Mo and W metals in chloroaluminate electrolytes, 3-electrode test cells were assembled with glassy carbon, Mo or W as working electrode and Al as counter and reference electrode. The chemical and electrochemical stability studies (see Supporting Information, Figure S4) of tungsten (W) and molybdenum (Mo) in 1.5 TEA electrolyte revealed that Mo has superior chemical and electrochemical stability in the electrolyte. Therefore, Mo was used as current collector in all the electrochemical characterisation experiments.

Electrochemical testing and measurements

Cyclic voltammetry experiments were carried out with a potentiostat/galvanostat (Parstat, AMETEK) in a 3-electrode cell configuration at a scan rate of 1 $mV\,s^{-1}$. The potential window was maintained between 0.5 to 2.5 V vs. Al/Al^{3+} and −0.3 to 1 V vs. Al/Al^{3+} for Al-graphite and Al-Al cells respectively. Galvanostatic cycling experiments were performed with a BioLogic BCS-810 battery testing system (Seyssinet-Pariset, France). Rate capability of cells was carried out at different current densities in the range of 0.1 to 5 $A\,g^{-1}$. The cut-off voltage of charging step was set to 2.4 and 2.45 V for the cells with 1.5 Emi and 1.5 TEA, respectively while cut-off voltage of discharging step was fixed to 0.4 V for both systems. The long-term cyclic stability of the cells was evaluated at 1 $A\,g^{-1}$. All measurements were performed at room temperature. All specific capacities are normalized to graphite mass.

Supporting Information

Supporting Information is available from the Wiley Online Library or from the author. Additional references cited within the Supporting Information.[36–38]

Acknowledgements

The authors would like to thank Beatriz Sanchez-Batalla from the DECHEMA research institute for performing physisorption measurements. The authors acknowledge the financial support provided by Federal Ministry of Education and Research (Grant No. 03SF0602A ALISS project and Grant No. 03XP0392C ALBATROS project). Open Access funding enabled and organized by Projekt DEAL.

Conflict of Interests

The authors declare no conflict of interest.

Data Availability Statement

The data that support the findings of this study are available from the corresponding author upon reasonable request.

Keywords: aluminium-ion battery · chloroaluminate electrolyte · ionic liquid · triethylamine hydrochloride

[1] P. K. Nayak, L. Yang, W. Brehm, P. Adelhelm, *Angew. Chem. Int. Ed.* **2018**, *57*, 102–120; *Angew. Chem.* **2018**, *130*, 106–126.
[2] G. A. Elia, K. Marquardt, K. Hoeppner, S. Fantini, R. Lin, E. Knipping, W. Peters, J.-F. Drillet, S. Passerini, R. Hahn, *Adv. Mater.* **2016**, *28*, 7564–7579.
[3] D. M. -Torrero, J. Palma, R. Marcilla, E. Ventosa, *Dalton Trans.* **2019**, *48*, 9906–9911.
[4] H. Yang, H. Li, J. Li, Z. Sun, K. He, H.-M. Cheng, F. Li, *Angew. Chem. Int. Ed.* **2019**, *58*, 11978–11996; *Angew. Chem.* **2019**, *131*, 12104–12124.
[5] H. Wang, Y. Bai, S. Chen, X. Luo, C. Wu, F. Wu, J. Lu, K. Amine, *ACS Appl. Mater. Interfaces.* **2015**, *7*, 80–84.
[6] S. Wang, S. Huang, M. Yao, Y. Zhang, Z. Niu, *Angew. Chem. Int. Ed.* **2020**, *59*, 11800–1180; *Angew. Chem.* **2020**, *132*, 11898–11905.
[7] T. Schoetz, B. Craig, C. P. Leon, A. Bund, M. Ueda, C. T. J. Low, *J. Energy Storage.* **2020**, *28*, 101176.
[8] M. C. Lin, M. Gong, B. Lu, Y. Wu, D.-Y. Wang, M. Guan, M. Angell, C. Chen, J. Yang, B.-J. Hwang, H. Dai, *Nature* **2015**, *520*, 324–328.
[9] W.-D. Pan, C. Liu, M.-Y. Wang, Z.-J. Zhang, X.-Y. Yan, S.-C. Yang, X.-H. Liu, Y.-F. Wang, D. Y. C. Leung, *Rare Met.* **2022**, *41*, 762–774.
[10] K. V. Kravchyk, M. V. Kovalenko, *Adv. Energy Mater.* **2019**, *9*, 1901749.
[11] K. V. Kravchyk, S. Wang, L. Piveteau, M. V. Kovalenko, *Chem. Mater.* **2017**, *29* (10), 4484–4492.
[12] D. Han, M.-S. Cao, N. Li, D.-M. She, W.-L. Song, H. Chen, S. Jiao, D. Fang, *Chin. J. Chem.* **2021**, *39*, 157–164.
[13] S. Wang, K. V. Kravchyk, F. Krumeich, M. V. Kovalenko, *ACS Appl. Mater. Interfaces* **2017**, *9*, 28478–28485.
[14] Z. Hu, H. Zhang, H. Wang, F. Zhang, Q. Li, H. Li, *ACS Materials Lett.* **2020**, *2*, 887–904.
[15] M. Angell, G. Zhu, M.-C. Lin, Y. Rong, H. Dai, *Adv. Funct. Mater.* **2020**, *30*, 1–11.
[16] F. Jach, M. Wassner, M. Bamberg, E. Brendler, G. Frisch, U. Wunderwald, J. Friedrich, *ChemElectroChem.* **2021**, *8*, 1988–1992.
[17] H. Xu, T. Bai, H. Chen, F. Guo, J. Xi, S. Cai, X. Chu, J. Ling, W. Gao, Z. Xu, C. Gao, *Energy Storage Mater.* **2019**, *17*, 38–45.
[18] K. L. Ng, T. Dong, J. Anawati, G. Azimi, *Adv. Sustainable Syst.* **2020**, *4*, 2000074.
[19] S. Xia, X. M. Zhang, K. Huang, Y.-L. Chen, Y. T. Wu, *J. Electroanal. Chem.* **2015**, *757*, 167–175.
[20] F. Gan, K. Chen, N. Li, Y. Wang, Y. Shuai, X. He, *Ionics* **2019**, *25*, 4243–4249.
[21] X. Dong, H. Xu, H. Chen, L. Wang, J. Wang, W. Fang, C. Chen, M. Salman, Z. Xu, C. Gao, *Carbon* **2019**, *148*, 134–140.
[22] H. Xu, H. Chen, H. Lai, Z. Li, Z. Dong, S. Cai, X. Chu, C. Gao, *J. Energy Chem.* **2020**, *45*, 40–44.
[23] R. J. Gale, R. A. Osteryoung, *Inorg. Chem.* **1980**, *19*, 2240–2242.
[24] T. Moumene, E. H. Belarbi, B. Haddad, D. Villemin, O. Abbas, B. Khelifa, S. Bresson, *J. Mol. Struct.* **2014**, *1065–1066*, 86–92.

[25] G. Socrates. *Infrared and Raman characteristic group frequencies. Tables and charts*. John Wiley and Sons, Ltd, Chichester, **2001**, p. 109.
[26] S. Guo, H. Yang, M. Liu, X. Feng, Y. Gao, Y. Bai, C. Wu, *ACS Appl. Mater. Interfaces* **2021**, *13*, 22549–22558.
[27] L. Zhang, L. Chen, H. Luo, X. Zhou, Z. Liu, *Adv. Energy Mater.* **2017**, *7*, 1–7.
[28] J. H. Xu, T. Schoetz, J. R. McManus, V. R. Subramanian, P. W. Fields, R. J. Messinger, *Electrochem. Soc. Interface* **2021**, *168*, 060514.
[29] N. P. Stadie, S. Wang, K. V. Kravchyk, M. V. Kovalenko, *ACS Nano* **2017**, *11*, 1911–1919.
[30] J.-J. Lee, I. T. Bae, D. A. Scherson, B. Miller, K. A. Wheeler, *J. Electrochem. Soc.* **2000**, *147*, 562.
[31] T. Jiang, M. J. Chollier Brym, G. Dubé, A. Lasia, G. M. Brisard, *Surf. Coat. Technol.* **2006**, *201*, 1–9.
[32] C.-J. Pan, C. Yuan, G. Zhu, H. Dai, *Proc. Natl. Acad. Sci. USA* **2018**, *115*, 5670–5675.
[33] G. A. Elia, I. Hasa, G. Greco, T. Diemant, K. Marquardt, K. Hoeppner, R. J. Behm, A. Hoell, S. Passerini, R. Hahn, *J. Mater. Chem. A* **2017**, *5*, 9682–9690.
[34] D. M-Torrero, P. Leung, E. G- Quismondo, E. Ventosa, M. Anderson, J. Palma, R. Marcilla, *J. Power Sources* **2018**, *374*, 77–83.
[35] Z. Li, J. Li, X. Li, W. Zhang, *J. Power Sources* **2020**, *467*, 228323.
[36] K. L. Ng, Z. Lu, Y. Wang, C. V. Singh, G. Azimi, *J. Phys. Chem. C* **2021**, *125*, 15145–15154.
[37] V. A. Elterman, P. Y. Shevelin, L. A. Yolshina, E. G. Vovkotrub, A. V. Borozdin, *J. Mol. Liq.* **2020**, *320*, 114482.
[38] A. A. Fannin Jr, D. A. Floreani, L. A. King, J. S. Landers, B. J. Piersma, D. J. Stech, R. L. Vaughn, J. S. Wilkes, J. L. Williams, *J. Phys. Chem.* **1984**, *88*, 2614–2621.

Manuscript received: February 3, 2023
Revised manuscript received: April 17, 2023
Version of record online: May 4, 2023